Long-term creep behavior of a short carbon fiber-reinforced PEEK at high temperature: Experimental and modeling approach

Sylvain Corveleyn, Frederic Lachaud, Florentin Berthet, Claude Rossignol

Long-term creep behavior of a short carbon fiber-reinforced PEEK at high temperature: Experimental and modeling approach

Sylvain Corveleyn [a], Frederic Lachaud [a,*], Florentin Berthet [a], Claude Rossignol [b]

[a] Institut Clément Ader (ICA), Université de Toulouse, CNRS UMR 5312-INSA-ISAE-Mines Albi-UPS, Toulouse, France
[b] LIEBHERR Aerospace, 408 Avenue des États Unis, 31016 Toulouse, France

Keywords:
PEEK
Short carbon fiber composite
Time-dependent mechanical behavior
TTSP
Maxwell Generalized model
Carbone-Peek Composite
Thermoplastic matrix composite
Visco-elastic behavior
Long term failure prediction

A B S T R A C T

In this work, the time-dependent mechanical behavior of a short carbon fiber-reinforced PEEK is investigated at temperatures near and above the glass transition temperature and for stresses below the damage threshold. An experimental procedure including creep/recovery tests and dynamic mechanical tests was carried out by varying stress levels, temperatures and fiber orientation. The mechanical behavior is shown to be linear viscoelastic below the damage threshold. Effect of the fiber orientation on elastic and viscoelastic behavior is similar. A procedure involving the time–temperature superposition principle (TTSP) is set to assess the long-term linear viscoelastic behavior and is shown to provide reliable results. A Maxwell Generalized model is used for unidirectional identification of the model's parameters. It is then implemented via a UMAT in Abaqus with failure criteria for viscoelastic materials from the literature for 3D calculation of industrial parts.

1. Introduction

Composite materials are increasingly used in the transport industry [1] as they possess high specific mechanical properties, fatigue properties compared to other materials such as metal alloys and are corrosion-free. As a result, the use of composite materials has grown over the past twenty years to lighten structures in the transport industry (for example, in aerospace with the A350, the Boeing 787 containing more than 50% by weight of composite materials or in the automotive industry with the BMW i3, whose body is entirely made of composite materials [2]). More specifically, thermoplastic based composites have sparked interest for some applications[3] because they have a short cycle time[4], they are weldable[5], have a better impact strength than thermoset based composites [6] and are mostly recyclable[7]. They allow production time and cost reductions compared to thermoset composite materials: for example, Fokker claims 20% cost and 10% mass savings on the fully thermoplastic composite elevators and rudder of its Gulfstream G650[8]. Some thermoplastics are considered as high-performance polymers (e.g. PPS, POM, PEI and PAEK) as they possess remarkable thermomechanical performance[9]. Their composites allow the production of lighter and less expensive parts than those produced from aluminum alloys. Their chemical resistance also allows the production of parts without any surface treatment[10].

Among these materials, carbon fiber-reinforced PEEK is interesting for applications requiring high thermomechanical properties [4,11]. Its physicochemical structure gives it chemical resistance over a broad range of fluids [10] and thermomechanical resistance with a high glass transition temperature (T_g = 143 °C), melting temperature (T_m = 343 °C) and high crystallization rate [12,13]. These properties make PEEK composites good candidates for use as structural materials, even for high temperatures [11]. Even though continuous carbon fiber-reinforced composites offer high mechanical performance, their manufacturing processes limit their use to simple geometries. The use of short carbon fiber-reinforced PEEK allows the design of complex geometries for semi-structural parts and the production of large series by injection molding.

At high temperatures however, typically higher than the glass transition temperature, semi-crystalline thermoplastic composites undergo creep (defined as time-dependent strain evolution under constant stress) [14]. Continuous carbon fiber-reinforced PEEK composites do not undergo creep when fibers are oriented in the load direction (only transverse or in-plane shear creep occurs with this type of composites) [15–17]. This is not the case for short carbon fiber-reinforced thermoplastic composites where creep occurs even in the fiber direction [18,19]. This phenomenon can lead to failure over extended periods [20,21], or make the part too deformed to be suitable for its intended

* Corresponding author.
E-mail address: frederic.lachaud@isae-supaero.fr (F. Lachaud).

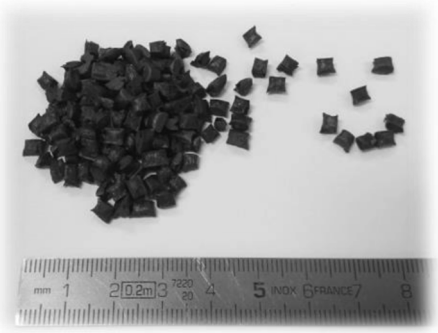

Fig. 1. Pellets of Victrex® PEEK 90HMF40.

use. Long-term creep behavior at temperatures higher than the glass transition temperature must be taken into account during the design stage of the part. Little is known, however, of the long-term creep behavior of this kind of material.

The time-dependent mechanical behavior type of study depends on the final application[15]. For high-temperature forming of thermoplastic composites, viscoplastic behavior will be used. For strain evolution until failure of materials under constant mechanical load, viscoelastic behavior is used. In this work, viscoelastic behavior will be studied. Viscoelasticity can be linear if there exists a linear relationship between stress and viscoelastic strain, or non-linear if this is not the case [15,16,22]. Viscoelasticity can be studied by dynamic mechanical testing[14,23,24], with creep/recovery tests [15,16,22,25] (static tests with imposed load) or relaxation tests (static test with imposed strain) [24]. Temperature has a great influence on time-dependent mechanical behavior due to macromolecular chain mobility changes[11,14,16]. Methods linking time to temperature allow long-term behavior determination with short-term tests[14,26]. Moreover, the mechanical behavior of short carbon fiber-reinforced composites is anisotropic [11,12] as is time-dependent mechanical behavior [18,19,27].

To model the viscoelastic behavior of materials, an empirical model as power law, also called Findley's law, has been used and extended to non-linear viscoelasticity [28]. Its time domain validity remains limited. Some rheological models based on assembly of springs and dashpots can be used for linear viscoelasticity behavior. The Zener model, also known as the standard generalized model, is a combination of a Maxwell model (consisting of a spring-dashpot in series) in parallel with a spring. As it possesses only one relaxation time, it is limited to simple cases and limited time periods. The Maxwell generalized model is a development of the Zener model with an unlimited number of Maxwell elements (spring-dashpot in series). It provides as many relaxation times as needed to take into account more precisely the complex mechanical behavior over a broader range of time[18,29,30]. The spectral model is also used to model the time-dependent mechanical behavior of composite materials. Relaxation times are linked to their weigh in the mechanical behavior via a distribution function (Gaussian function for example). This allows modeling with a limited number of parameters and has been mostly used for laminated composites[15,16]. Introducing non-linear parameters adapts the model to nonlinear viscoelasticity. To take into account time-dependent failure, some failure criteria of viscoelastic materials have already been compared to experimental viscoelastic failure data obtained on glass/epoxy composites leading to good predictions [20,21,31].

The objective of this work is to study the time-dependent mechanical behavior of a short carbon fiber-reinforced PEEK over a very long time period (at least several decades) and at temperatures higher than T_g for a potential industrial application at these high temperatures. The work is split into two parts:

- an experimental investigation of time-dependent mechanical behavior of the material to define its mechanical behavior and limits of its use
- a modeling study intended to propose a mechanical model of the time-dependent behavior with associated failure criteria, to identify it and to simulate the behavior and time-dependent failure of structures at high temperatures.

2. Experimental study

The purpose of the experimental study of the material's time-dependent mechanical behavior is to investigate the effect of stress applied, temperature and fiber orientation. The experimental procedure described below will vary all these parameters in order to define a mechanical model and to identify its parameters.

2.1. Material and process

The material used in this study is an easy flow grade of PEEK reinforced with 40% by weight short high-modulus carbon fibers (with a mean length of 120 μm [12]) provided by Victrex® as pellets under commercial name PEEK 90HMF40 (Fig. 1). The samples used in this study are injection molded dumbbell samples according to ISO527 1A and dumbbell samples machined from injection molded plates according to ISO527 1BA (Fig. 2). Dumbbell samples and plates were injection molded with a DK 65/160 machine with parameters shown Table 1.

Fiber orientation in the material is checked by microscopic observations of a cut specimen (Fig. 3). The common core/shell structure is observed with fibers oriented along the direction of injection near the surface (shell) and a core, with fibers oriented perpendicular to the injection direction [32]. The shell is thicker than the core and fibers are mostly aligned in the injection direction. This is explained by the flow during injection: near to the mold surface, shear flow aligns fibers into the direction of injection, while far from the mold surface, elongational flow aligns fibers perpendicular to the injection direction [32]. To study the effect of fiber orientation on mechanical behavior, ISO527-1BA samples were machined from injected plates at 0°, 45° and 90° from the injection direction. Shear flow occurring on mold cavity also explains why ISO527-1A samples have more fibers oriented in the injection direction than ISO527-1BA samples cut in the injection direction from plate (see Fig. 4).

2.2. Experimentation campaign

An experimental procedure including static tensile tests, creep/recovery tests and dynamic mechanical tests is carried out. The aim is to define the stress range (situated below the damage threshold), time-dependent mechanical behavior and to provide long-term experimental data for the modeling study. The influence of stress, temperature and fiber orientation is investigated.

2.2.1. Short-term creep test

Prior to the creep tests, the stress range for material use must be determined and, specifically, the maximum stress defined here as stress value when damage begins to appear. The material is mechanically characterized in traction at room temperature, 150 °C and 250 °C with both monotonic and loading/unloading tests (an example of curves at 150 °C on an ISO527-1A sample is given Fig. 5) at strain rate $\dot{\varepsilon} = 10^{-4}s^{-1}$. The machine used is an INSTRON 8862 and strain is measured with an extensometer 2620–601 having a 25 mm gauge length. In this manner, the engineering properties (elastic modulus, strain and stress at failure) as well as plasticity and damage can be measured. Plasticity is defined as the permanent strain after unloading (Fig. 5). Damage is defined as the drop in material rigidity and computed as Eq. (1).

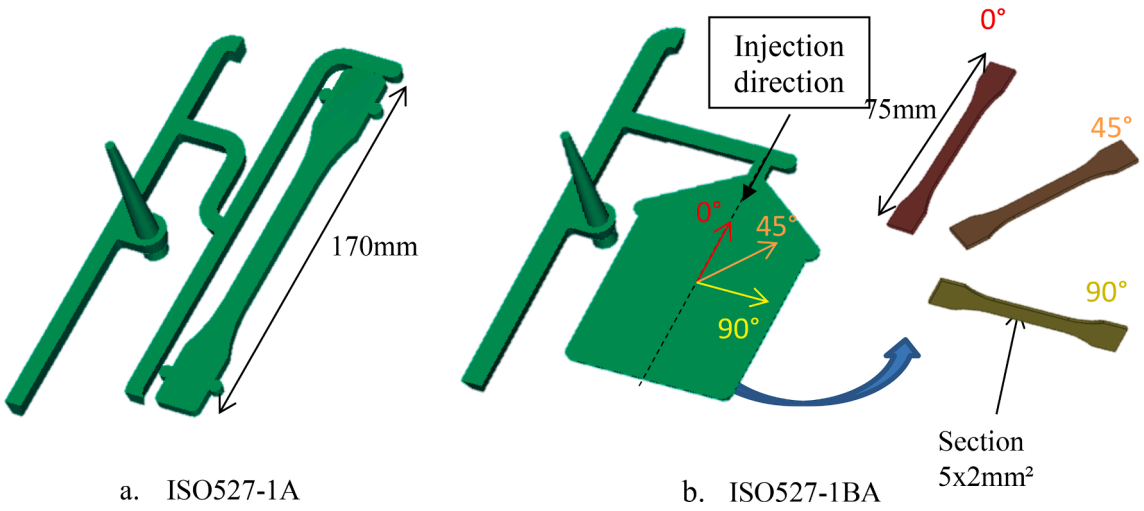

Fig. 2. Injection molded samples used for the tensile creep study.

Table 1
Injection parameters used for injection molding the samples of this study.

T_{melt} (°C)	420
T_{mold} (°C)	200
P_{hold} (MPa)	80
t_{hold} (s)	12
t_{cool} (s)	55

$$d_i = 1 - \frac{E_i}{E_1} \quad (1)$$

Where E_i is the secant modulus obtained on the i^{th} loading/unloading cycle and E_1 is obtained in the elastic part of the traction curve (graphical explanation is given Fig. 5).

At least 3 samples are tested, including at least 2 for loading/unloading tests. Example of results obtained at 150 °C are shown in Fig. 5 (note that damage and plasticity are determined by the stress levels chosen) and some engineering properties are summarized in Table 2. The quasi-static mechanical behavior of the material is seen to be temperature-dependent: brittle below T_g and softer and more ductile above. This behavior is linked to the semi-crystalline nature of the PEEK matrix.

From damage evolution (like that shown Fig. 5 for an ISO527-1A sample tested at 150 °C), a maximum stress for use of material for each type of configuration (temperature, fiber orientation) is set, as shown in Table 3. This value corresponds to the damage threshold of the material and stresses below this value are assumed to not damage the material.

Material creep is studied in traction at room temperature, 150 °C and 250 °C and under stresses below the damage threshold following the quasi-static mechanical characterization presented before. An MTS tensile machine is used, and strain is measured with either an extensometer 634.33F-01 having a 25 mm gauge length, or a strain gage which provides better results (no sliding and better accuracy). Viscoelastic behavior is identified with a multi-step creep/recovery test procedure including 5 creep/recovery steps with increasing load (Fig. 6) [22]. Loading rate is set to 1 MPa.s^{-1}, creep steps are 4 h long and recovery steps are 8 h long.

2.2.2. *Long-term creep test based on DMA*

The aim is to identify long-term creep compliance by applying the time–temperature superposition principle (TTSP) to linear viscoelastic properties[14,26]. Tests are carried out with ISO527-1A sample in traction on a BOSE ELECTROFORCE 3330 A-T (Fig. 7). Strain is measured with strain gages.

A frequency and temperature sweep is used in the experiment. Frequency is varied from 0.02 Hz to 22 Hz and temperatures at 40 °C and from 100 °C to 310 °C every 10 °C. Amplitude is chosen as 0.05 mm in order to remain within the hypothesis of linear viscoelasticity. Vertical shift is applied to the storage modulus master curve to match the storage modulus at 40 °C to the modulus measured by tensile traction tests at

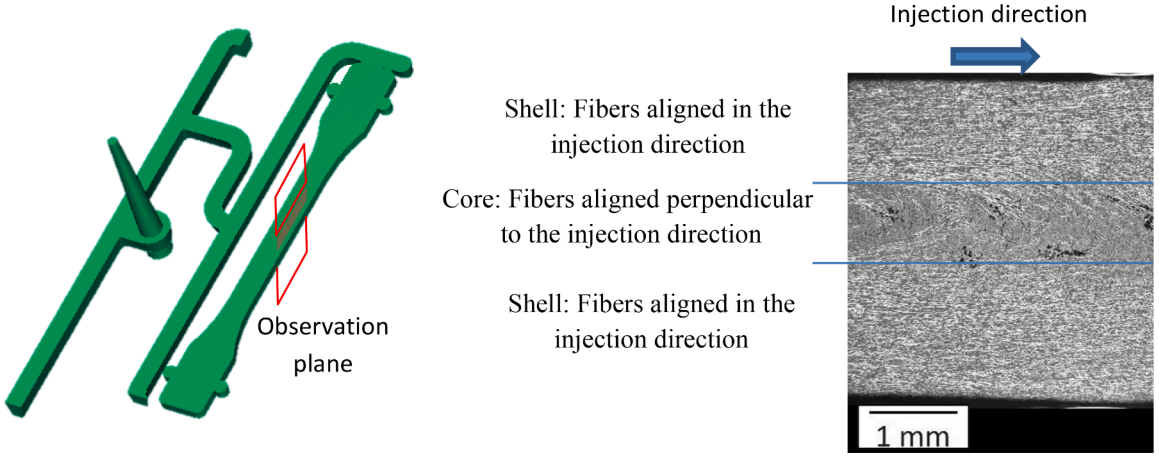

Fig. 3. Microscopic observations made on the ISO527 1A sample.

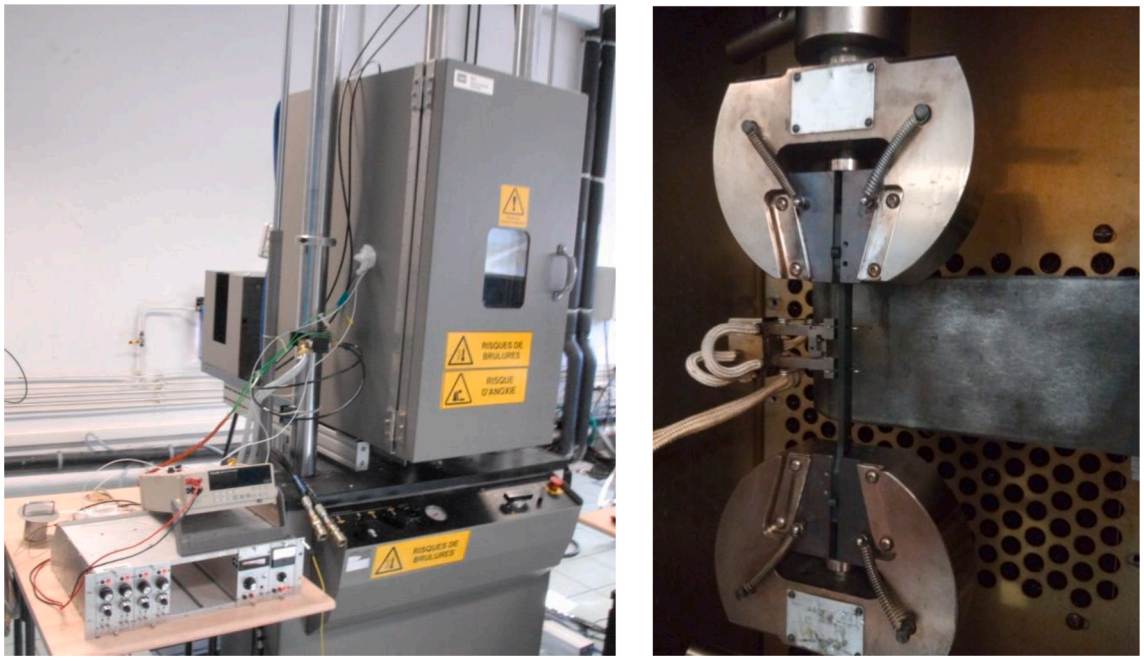

Fig. 4. Experimental setup for monotonic, loading/unloading traction tests.

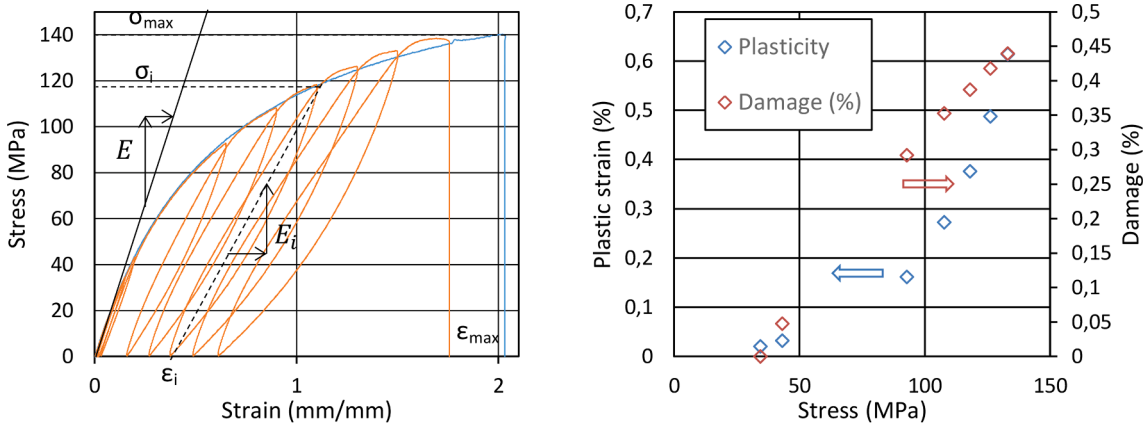

a. Stress/strain behavior b. Plasticity and damage evolution

Fig. 5. Monotonic and loading/unloading at 150 °C on an ISO527-1A sample.

Table 2
Engineering properties measured on 4 samples at room temperature, 150 °C and 250 °C on ISO527-1A samples.

Test temperature	Elastic modulus (MPa)		Stress at failure (MPa)		Strain at failure (%)	
	Mean	Standard deviation	Mean	Standard deviation	Mean	Standard deviation
25 °C	40,937	1470	295	6,00	1.08	0.03
150 °C	19,825	1137	141.4	3.5	2.13	0.31
250 °C	13,322	1942	85.0	1.88	2.85	0.23

Table 3
Damage threshold function of sample type and temperature.

Temperature	Sample	Damage threshold (MPa)
23 °C	ISO527-1A	100
	ISO527-1BA cut at 0°	100
	ISO527-1BA cut at 45°	50
	ISO527-1BA cut at 90°	50
150 °C	ISO527-1A	40
	ISO527-1BA cut at 0°	40
	ISO527-1BA cut at 45°	30
	ISO527-1BA cut at 90°	25
250 °C	ISO527-1A	25
	ISO527-1BA cut at 0°	25
	ISO527-1BA cut at 45°	15
	ISO527-1BA cut at 90°	15

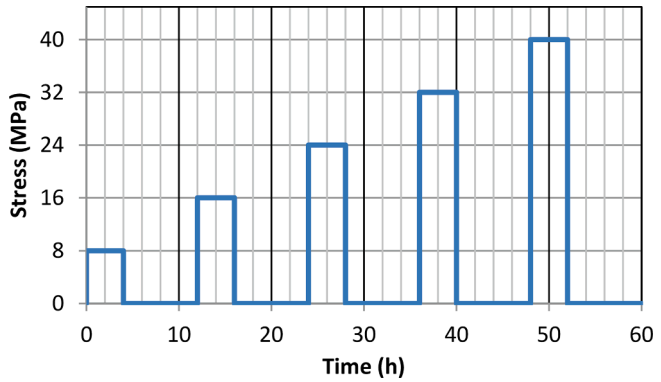

Fig. 6. Multi-step creep/recovery test procedure (example for test on ISO257-1A sample at 150 °C).

room temperature [33].

2.3. Results and discussion

2.3.1. Short-term creep tests

The raw results for creep/recovery tests of an injection molded dumbbell sample at 150 °C are shown Fig. 8. An average curve (arithmetic mean of all samples tested) is also shown. The results show that there is residual strain at the end of the recovery step which can be due to plastic deformation or material aging.

Another mechanical loading history was applied and shows (Fig. 9) that after having been stressed at the maximum stress, the residual strain after recovery does not change during the remainder of the test. This shows that residual strain is due to plasticity.

Viscoelastic strain during creep steps is extracted from raw results subtracting elastic and plastic strain from the total strain measured as viscoplastic strain is shown to not appear. It is then possible to determine whether viscoelasticity is linear or not. Fig. 10 shows creep compliance computed as Eq. (2) during each i^{th} creep step for the test carried out at 150 °C and an average of the five curves smoothed with a moving average.

$$\mathbf{C}_i(t) = \frac{\boldsymbol{\varepsilon}_{visco}(\boldsymbol{\sigma}_i, t)}{\boldsymbol{\sigma}_i} \tag{2}$$

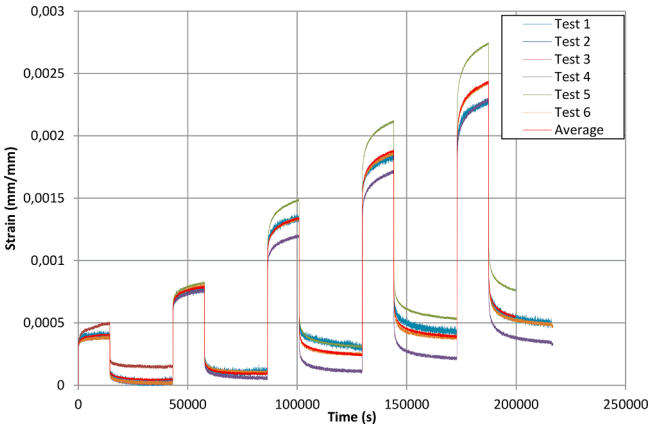

Fig. 8. Experimental results obtained for several creep/recovery tests on ISO527-1A samples.

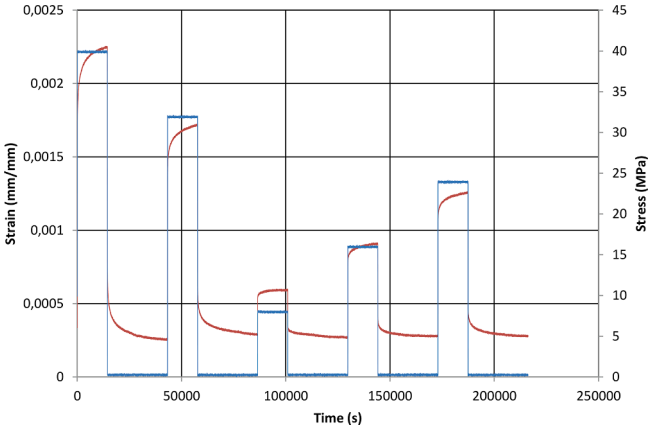

Fig. 9. Mechanical history shows plasticity is the cause of permanent strain on an ISO527-1A sample.

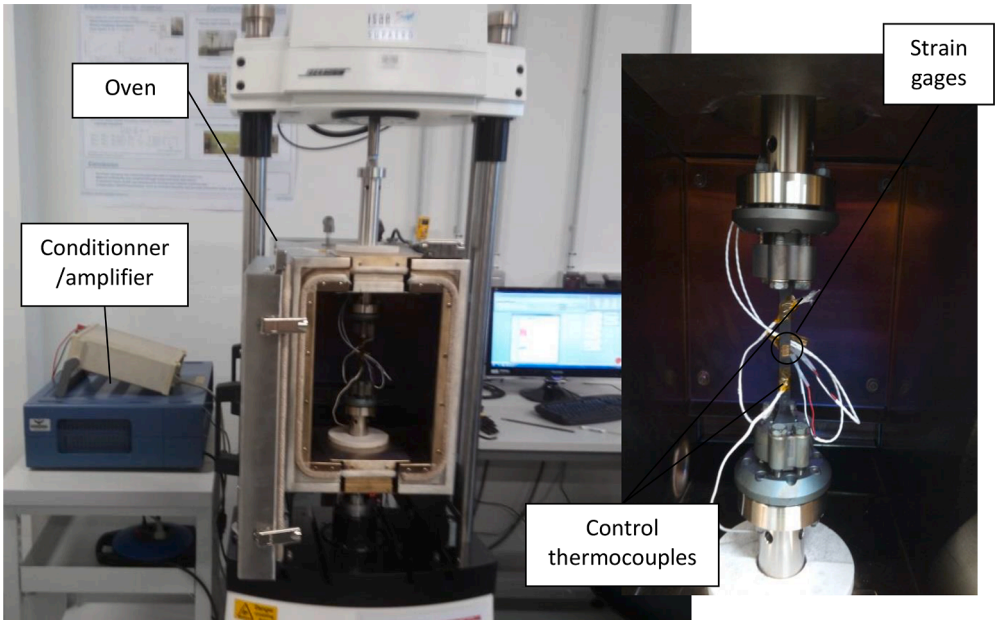

Fig. 7. Experimental setup for mechanic dynamical tests in traction.

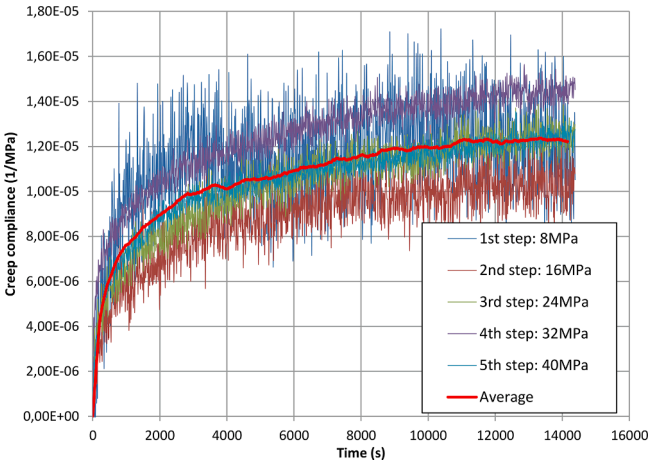

Fig. 10. Creep compliance during creep steps for the different magnitude of stress on ISO527-1A samples.

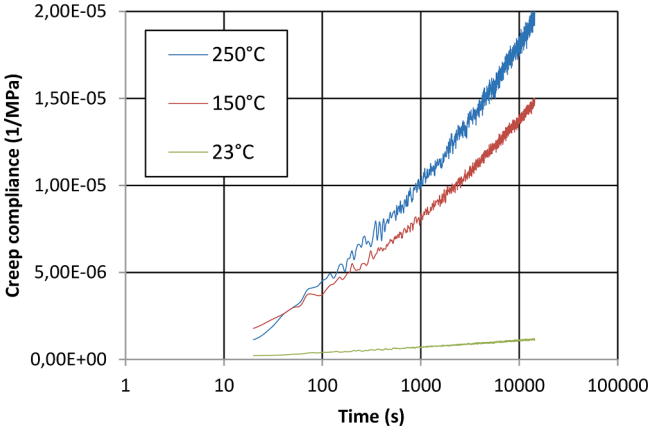

Fig. 11. Creep compliance obtained at room temperature, 150 °C and 250 °C on an injection molded ISO 527-1A sample.

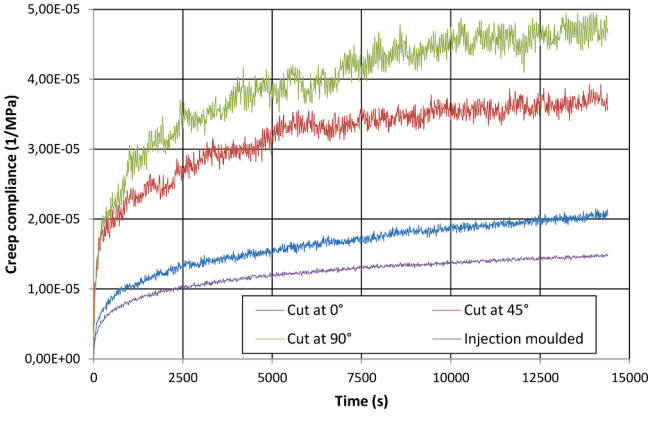

Fig. 12. Effect of fiber orientation on creep compliance.

Where $C_i(t)$ is the time-dependent creep compliance, $\varepsilon_{visco}(\sigma_i, t)$ is the time-dependant viscous strain and σ_i the stress applied during each i^{th} creep step.

The five curves show a satisfactory overlap (Fig. 10). Hence, viscoelasticity can be considered linear below the damage threshold. The same observations are made with tests at room temperature and 250 °C.

Similar calculations can be performed on results obtained at room temperature and 250 °C. Creep compliance values for the three temperatures of interest are shown Fig. 11. Almost no creep occurs at room temperature: viscoelastic strain after 4 h creep is 10^{-6}. However, at 150 °C and 250 °C, creep is greater and varies with temperature: the higher the temperature, the larger the creep strain (viscoelastic strain after 4 h creep is 1.5 10^{-5} at 150 °C and 1.9 10^{-5} at 250 °C). This can be explained because the glass transition temperature of PEEK is 143 °C: at room temperature, the material is in its glassy state and only little macromolecular movement can occur. At 150 °C and 250 °C, corresponding to the end of transition to the rubbery state, macromolecular chain movement is allowed in the amorphous phase of the polymer. Finally, creep compliance appears quite linear in the log(time) scale, which means that an exponential law can properly describe the creep compliance function of time within the test time.

Due to the molding process, fiber orientation leads to an anisotropic elastic behavior[12] and viscoelasticity should also be anisotropic. Creep compliances measured for the different material orientations are shown Fig. 12. Viscoelastic strain is smaller as the fibers are oriented in the load direction. More waviness for the 90° and 45° curves can be noticed as the stress involved to test these samples is smaller than for the 0° and injection molded samples and considering the compliance definition shown Eq (2).

Fig. 13 shows that there is a linear relationship between creep compliance and elastic modulus: creep compliance divided by the elastic modulus function of the different fiber orientations appear similar given experimental uncertainties existing in stress/strain measurements. This is observed whatever the temperature (150 °C or 250 °C). Linear viscous mechanical behavior is due to the matrix and the influence of fibers is similar in elasticity and linear viscoelasticity[27].

With short-term creep tests, the effect of stress level, fiber orientation and temperature were investigated. The time-dependent mechanical behavior of the studied material is shown to be linear viscoelastic below the damage threshold. There is almost no creep at room temperature, but above the glass transition temperature, viscous behavior is observed. Finally, fiber orientation has the same influence on viscoelasticity as on elasticity.

2.3.2. *Long-term creep tests*

The modulus function of frequency and temperature obtained by DMA tests is shown Fig. 14 aFigure **14**. For temperatures below 120 °C, the effect of frequency on the modulus is limited (1.2% decrease in modulus). This can be explained by the reduced mobility of the macromolecular chains below Tg-30 °C for most polymers [34]. At the glass transition temperature, the material undergoes the biggest decrease in modulus (19GPa drop between 120 °C and 190 °C).

A master curve of the modulus can be then obtained by horizontally shifting the curves from one reference curve. This is also known as the Time Temperature Superposition Principle (TTSP)[14] and can be formalized as Eq. (3):

$$E(t,T) = E(\frac{t}{a_T}, T_0) \tag{3}$$

Where E is the modulus, t the time, T the temperature, T_0 the reference temperature and a_T the shifting factor. The shifting factor experimentally obtained can be linked with temperature through Arrhenius' law[14] as Eq. (4):

$$log(a_T) = \frac{E_a}{2,3 \times R} \times \left(\frac{1}{T} - \frac{1}{T_0}\right) \tag{4}$$

Where R is the perfect gas constant and E_a is the activation energy to be defined. This activation energy is the only parameter linking time and temperature in the viscous behavior.

The reference temperature is chosen to be 120 °C because it corresponds to the onset of the thermomechanical curve. By horizontally shifting the curves obtained for each other single temperature (higher temperatures to lower frequencies), the smooth master curve for a reference temperature of 120 °C shown Fig. 14 b. is created.

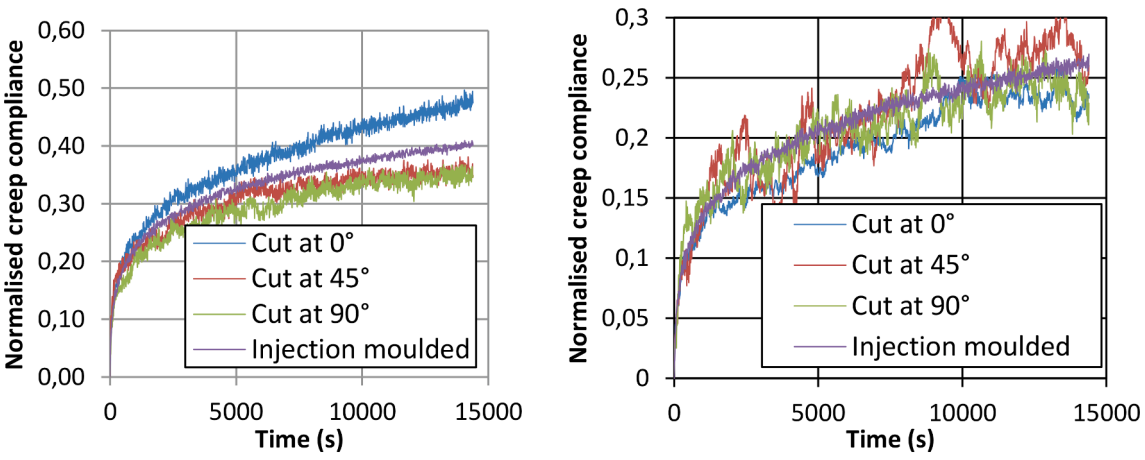

a. 150°C

b. 250°C

Fig. 13. Creep compliance normalized to tensile modulus shows that there is a similar effect of the fiber orientation on elastic and viscoelastic behavior at 150 °C and 250 °C.

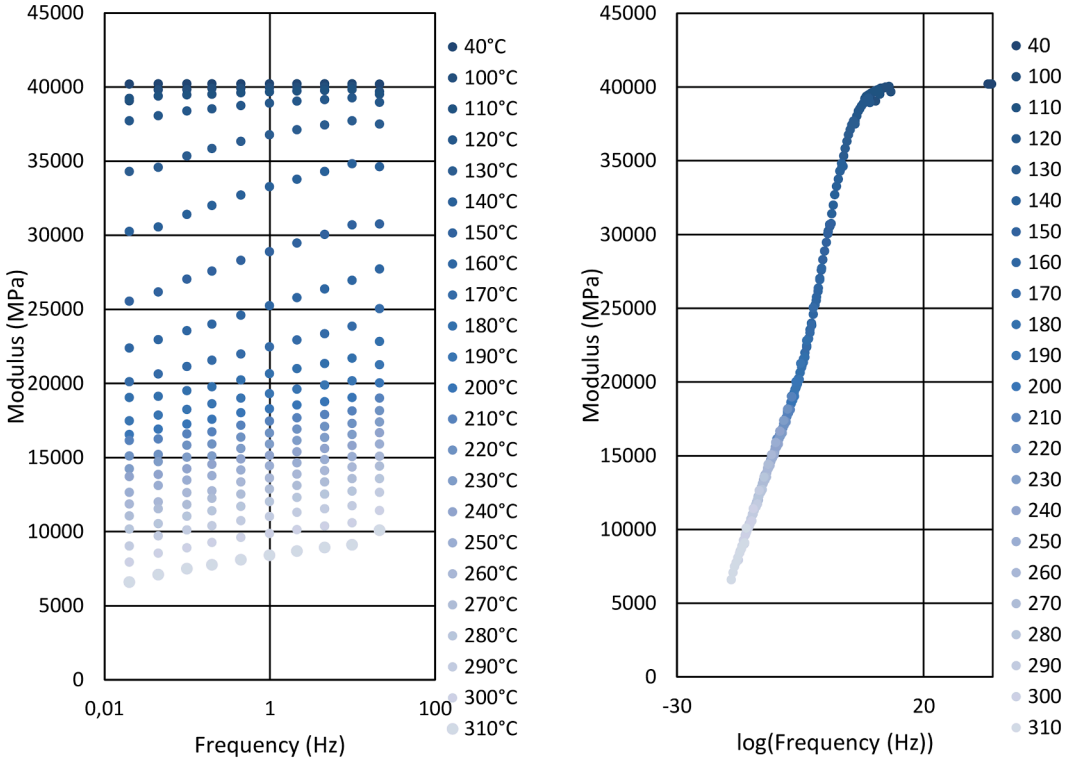

a. Raw results

b. Master curve obtained after TTSP horizontal shifting with a reference temperature of 120°C

Fig. 14. Raw results of DMA test and master curve.

The Arrhenius plot of the shift factor (Fig. 15) shows a satisfactory linearity $R^2 = 0.98$ and activation energy is calculated as 515 kJ.mol^{-1}.

Modulus as a function of frequency obtained by DMA (master curve shown Fig. 15.b) can lead to creep compliance as a function of time following equations by Cai *et al.* [23] reminded Eq. (5).

$$\begin{cases} E(t) = E\left(\frac{1}{f}\right) \\ D(t) = \frac{1}{E(t)} \end{cases} \quad (5)$$

In this way, the data obtained by both short-term and long-term creep tests can be compared. Fig. 16 shows satisfactory trends of those

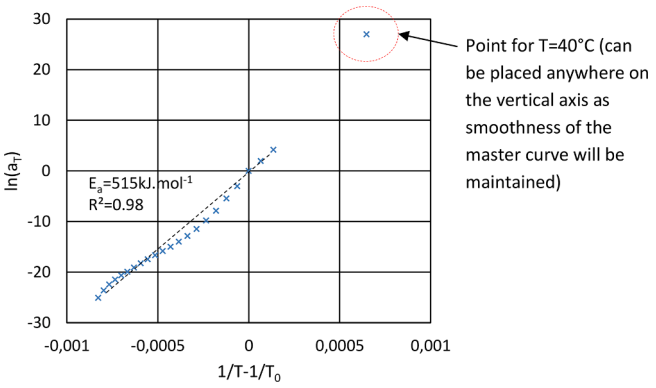

Fig. 15. Arrhenius plot of the shift factor for a reference temperature of 120 °C.

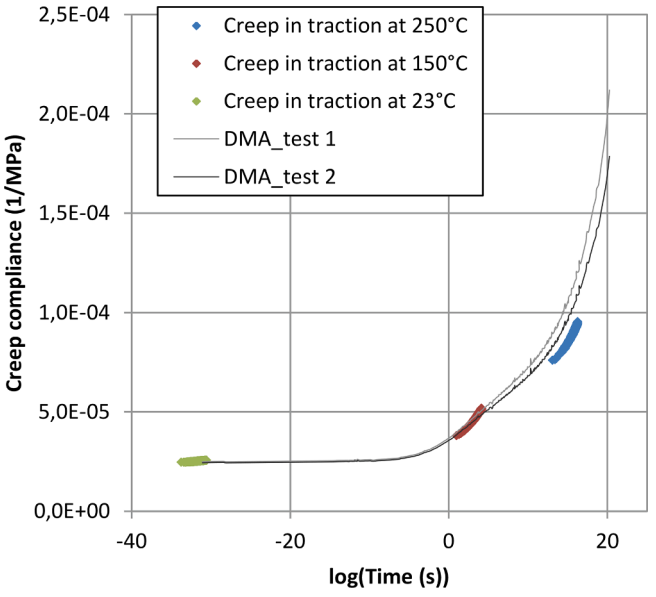

Fig. 16. Effect of temperature on the creep compliance master curve.

data proving consistency of the method used.

The TTSP applied in our study provides long-term creep data for the material and the link between time and temperature. Data of long-term and short-term creep tests are consistent and provide confidence in the method used.

3. Modeling

The experimental study has provided data on the time-dependent mechanical behavior of short carbon fiber PEEK. Time-dependent mechanical behavior is linear viscoelastic below the damage threshold. The effects of temperature and fiber orientation have been determined. Finally, long-term data have been obtained as well as the relationship between time and temperature.

3.1. Creep model

In order to model the experimental mechanical behavior over a long time period, the Generalized Maxwell model is used (Fig. 17). It is a linear viscoelastic model comprised of springs and dashpots like other linear viscoelastic models such as the Maxwell model (comprised of a spring and a dashpot in series), the Voight model or the Zener model. The main advantage of the Generalized Maxwell model is that it considers relaxation times as necessary to describe the behavior of the material. The number of relaxation times is dependent upon the identification time considering that generally, one relaxation time per decade is used.

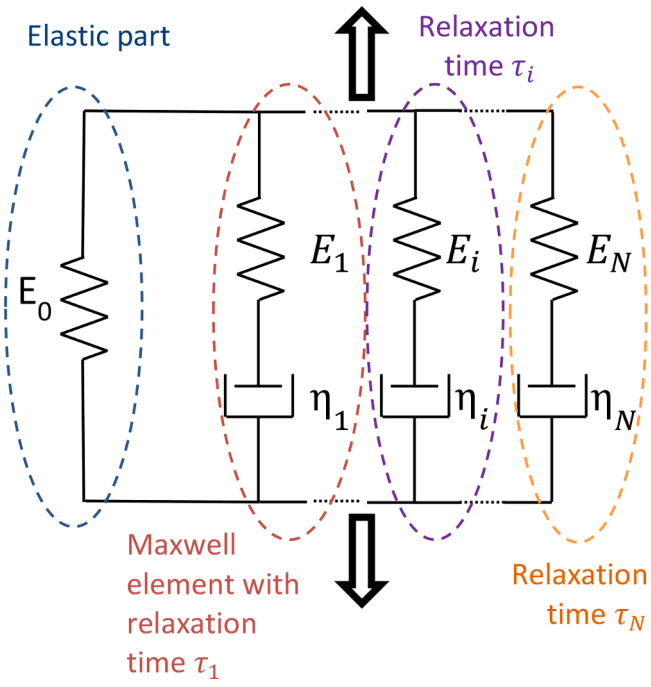

Fig. 17. . Generalized Maxwell model.

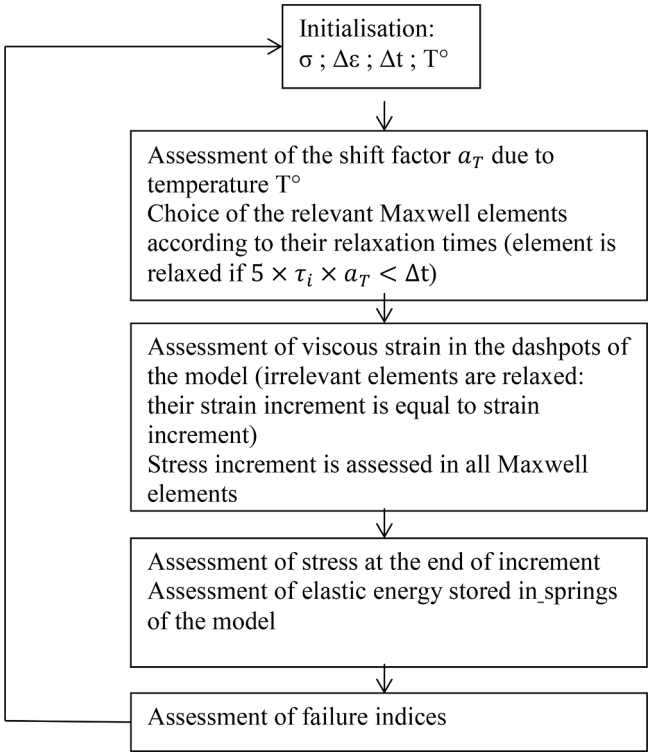

Fig. 18. Algorithm for calculation of a 3D part.

3.1.1. Hereditary equation for 1D modeling

To model the unidirectional behavior of a nonlinear viscoelastic material, Schapery's equation is commonly used [16,22,25,29,35]:

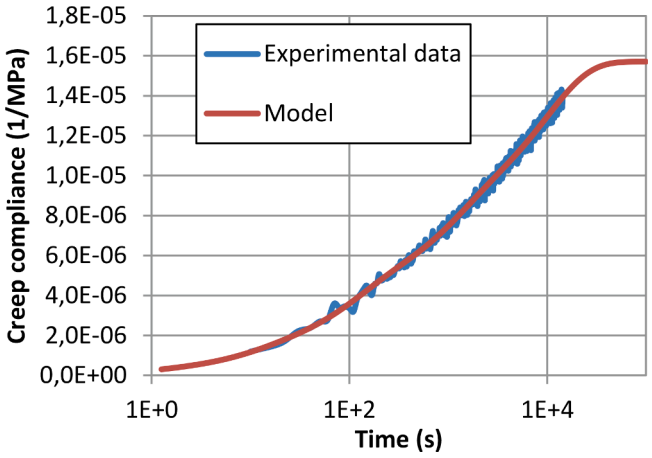

Fig. 19. Short-term identification of the model.

Table 4
Parameters identified.

τ_i(s)	D_i(1/MPa)
0	3,57E-05
1	2,04E-07
10	9,87E-07
100	3,09E-06
1000	3,92E-06
10,000	7,50E-06

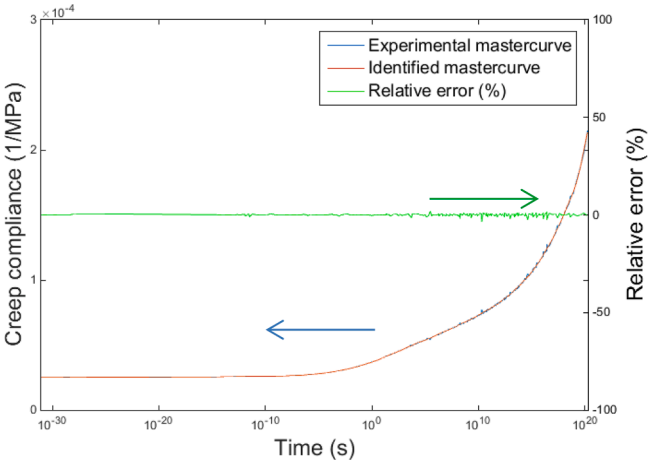

Fig. 20. Long-term identification.

$$\varepsilon(t) = g_0.D_0.\sigma(t) + g_1.\int_0^t \Delta D(\Psi - \Psi').\frac{d(g_2\sigma)}{d\tau}d\tau \tag{6}$$

Where D_0 is the elastic compliance and ΔD the transient compliance and.

$\Psi = \int_0^t \frac{dt'}{a_\sigma}$ and $\Psi' = \int_0^\tau \frac{dt'}{a_\sigma}$ are the reduced times andg_0,g_1, g_2 and a_σ are non-linear parameters which depend on the stress applied. If the material behaves linear viscoelastically, non-linear parameters are reduced to 1 and the equation becomes:

$$\varepsilon(t) = D_0.\sigma(t) + \int_0^t \Delta D(t-\tau).\frac{d\sigma}{d\tau}d\tau \tag{7}$$

Moreover, transient compliance is often described as a Prony series which considers relaxation times as necessary to properly describe the material's behavior:

$$\Delta D(t) = \sum D_i\left(1 - \exp\left(\frac{-t}{\tau_i}\right)\right) \tag{8}$$

Where D_i is the transient compliance associated with the relaxation timeτ_i.

Eqs. (7) and (8) correspond to the Generalized Maxwell model and the relationship with the notations shown Fig. 17 are reminded Eq. (9).

$$\begin{cases} E_j = \dfrac{1}{\sum_{i=0}^{j-1} D_i} - \dfrac{1}{\sum_{i=0}^{j} D_i} \\ \tau_i = \dfrac{\eta_i}{E_i} \\ \sum_{i=0}^{N} E_i = \dfrac{1}{\sum_{i=0}^{N} D_i} \end{cases} \tag{9}$$

To consider the effects of temperature, moisture and aging on viscoelastic behavior, reduced times are used and the previous equation (Eq. (7)) becomes:

$$\varepsilon(t) = D_0.\sigma(t) + \int_0^t \Delta D(\Psi - \Psi').\frac{d\sigma}{d\tau}d\tau \tag{10}$$

With $\Psi = \int_0^t \frac{dt'}{a_T.a_H.a_{te}}$ and $\Psi' = \int_0^\tau \frac{dt'}{a_T.a_H.a_{te}}$ the reduced times where a_T is the horizontal shift factor due to temperature, a_H the one linked to water uptake and a_{te} the one for aging. In this study, only the effect of temperature will be taken into account [15,29,36,37].

3.1.2. *Differential equation for 3D modeling*

The model by Vidal-Sallé and Chassagnes is used for 3D modeling of the viscoelastic behavior [30]. The constitutive equations are reminded in Eq. (11).

$$\begin{cases} \widetilde{\sigma} = \widetilde{\sigma}_0 + \sum_{i=1}^{N} \widetilde{\sigma}_i \\ \dot{\widetilde{\varepsilon}} = \widetilde{\widetilde{C}}_0\dot{\widetilde{\sigma}}_0 + \sum_{i=1}^{N} \widetilde{\widetilde{C}}_i\dot{\widetilde{\sigma}}_i + \widetilde{\widetilde{\Gamma}}_i\widetilde{\sigma}_i \end{cases} \tag{11}$$

Where $\widetilde{\sigma}$ is the total stress applied, $\widetilde{\sigma}_0$ is the stress applied to the spring branch and $\widetilde{\sigma}_i$ is the stress applied to the i^{th} Maxwell element, $\widetilde{\widetilde{C}}_0$ is the instantaneous stiffness matrix and $\widetilde{\widetilde{C}}_i$ and $\widetilde{\widetilde{\Gamma}}_i$ are the stiffness and viscous matrices of the i^{th} Maxwell element.

Elastic and viscoelastic stiffness matrices have the same material symmetry, as shown in Eq. (12).

$$\widetilde{\widetilde{\Gamma}}_i = \widetilde{\widetilde{C}}_i : \widetilde{\widetilde{\Theta}}_i$$

$$= A_i \begin{bmatrix} \frac{1}{E_1} & -\frac{\nu_{21}}{E_2} & -\frac{\nu_{31}}{E_3} & 0 & 0 & 0 \\ -\frac{\nu_{12}}{E_1} & \frac{1}{E_2} & -\frac{\nu_{32}}{E_3} & 0 & 0 & 0 \\ -\frac{\nu_{13}}{E_1} & -\frac{\nu_{23}}{E_2} & \frac{1}{E_3} & 0 & 0 & 0 \\ 0 & 0 & 0 & \frac{1}{G_{12}} & 0 & 0 \\ 0 & 0 & 0 & 0 & \frac{1}{G_{13}} & 0 \\ 0 & 0 & 0 & 0 & 0 & \frac{1}{G_{23}} \end{bmatrix} \begin{bmatrix} \frac{1}{\tau_1} & \frac{1}{\tau_7} & \frac{1}{\tau_8} & 0 & 0 & 0 \\ \frac{1}{\tau_7} & \frac{1}{\tau_2} & \frac{1}{\tau_9} & 0 & 0 & 0 \\ \frac{1}{\tau_8} & \frac{1}{\tau_9} & \frac{1}{\tau_3} & 0 & 0 & 0 \\ 0 & 0 & 0 & \frac{1}{\tau_4} & 0 & 0 \\ 0 & 0 & 0 & 0 & \frac{1}{\tau_5} & 0 \\ 0 & 0 & 0 & 0 & 0 & \frac{1}{\tau_6} \end{bmatrix} \tag{12}$$

3.2. *Implementation and identification*

3.2.1. *1D model: Simplification for viscoelastic model parameter identification*

Identification of the parameters for the viscoelastic model is carried out from the unidirectional tests presented below. Experimental results show that mechanical behavior is linear viscoelastic. Viscoelastic strain

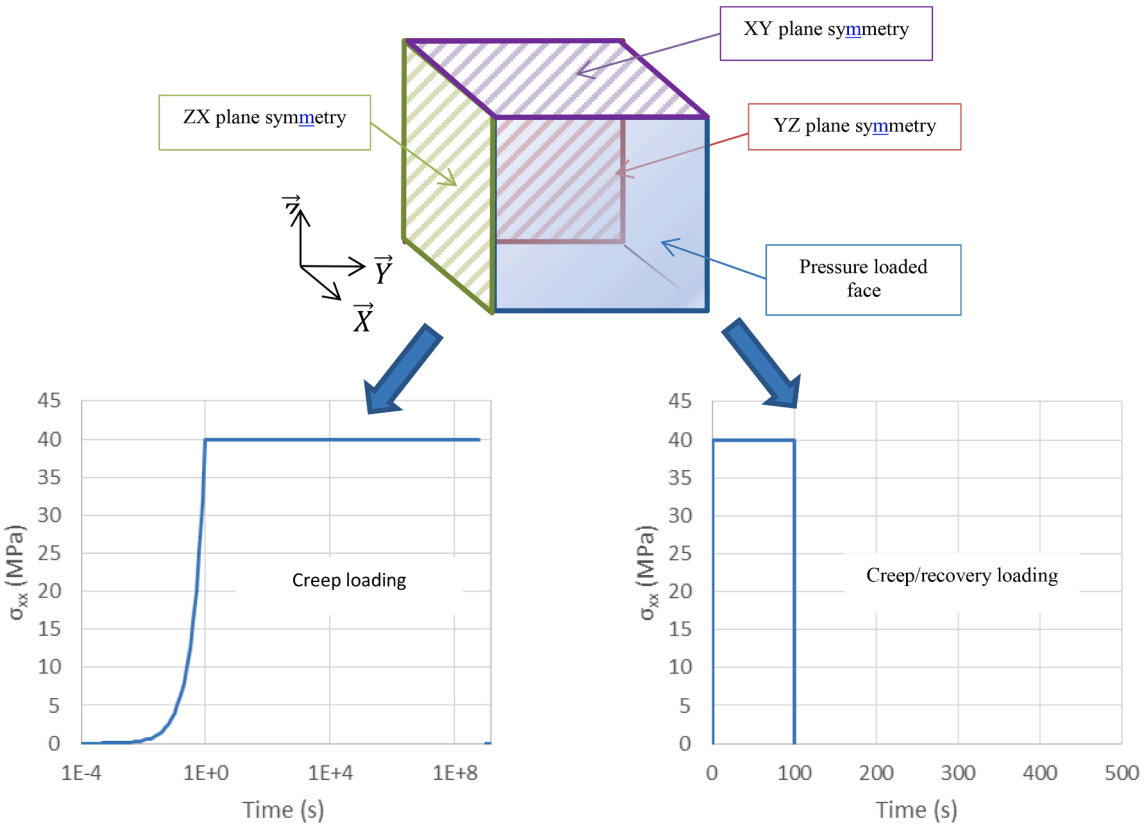

Fig. 21. Loading and limit conditions on a single element for model validation.

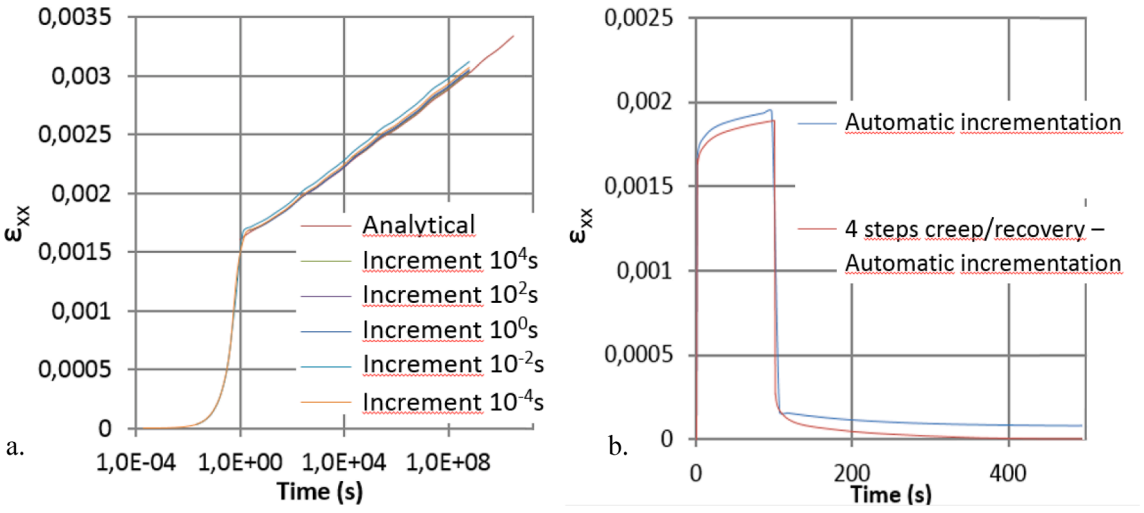

Fig. 22. Validation of model with pure creep (a.) and creep/recovery (b.).

can be described as follows, combining Eqs. (7) and (8).

$$\varepsilon(t) = D_0.\sigma_{11}(t) + \int_0^t \sum \frac{D_i}{\tau_i}.\exp\left(\frac{\tau - t}{\tau_i}\right).\sigma_{11}(t)d\tau \tag{13}$$

Eq. (13) can be written as the dot product shown Eq. (14).

$$\varepsilon(t) = \begin{pmatrix} \sigma_{11}(t) & C_1(t) & \cdots & C_i(t) & \cdots & C_N(t) \end{pmatrix} \begin{pmatrix} D_0 \\ D_1 \\ \vdots \\ D_i \\ \vdots \\ D_N \end{pmatrix} \tag{14}$$

The second vector is the one to be identified. The first one is fully defined as C_i are time-dependent and can be written for each time step as follows:

$$C_i(t+\Delta t) = \tau_i.\left[\frac{\Delta t}{2}.\left(\exp\left(-\frac{\Delta t}{\tau_i}\right).\sigma_{11}(t) + \sigma_{11}(t + \Delta t)\right) + C_i(t).\exp\left(-\frac{\Delta t}{\tau_i}\right)\right] \tag{15}$$

3.2.2. 3D model: Simplification and resolution for simulation

Once the parameters have been identified, carrying out any simulation on an industrial part needs to implement a 3D mechanical model.

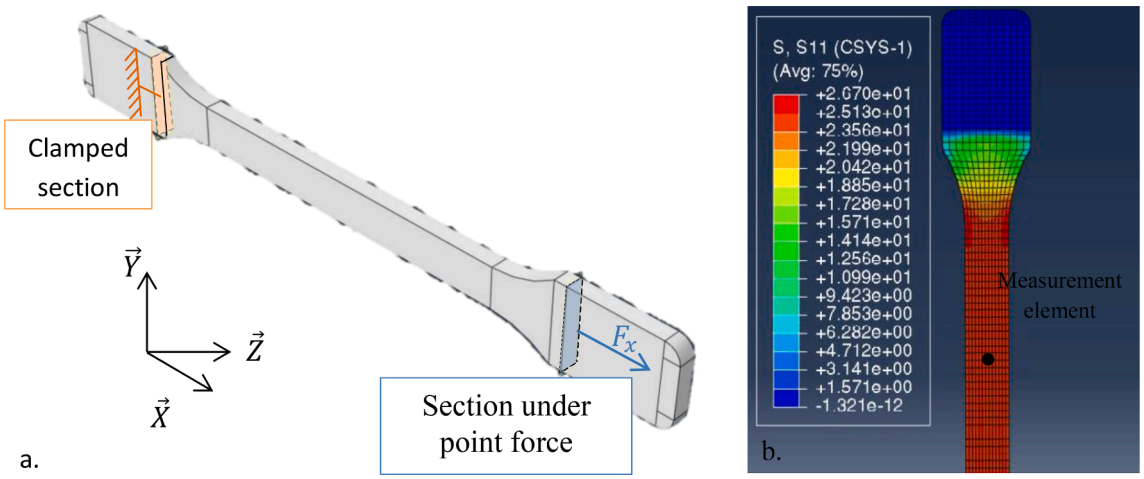

Fig. 23. Boundary conditions (a.) and tensile stress result (b.).

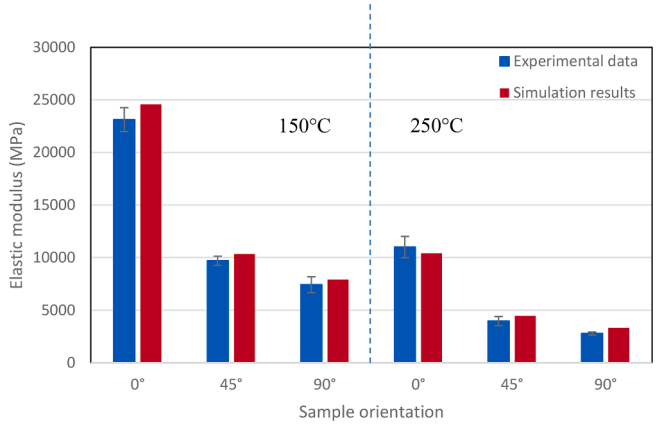

Fig. 24. Experimental and simulation comparison of elastic modulus for different temperatures and orientations.

According to the literature on elastic behavior[12] and experimental results on time-dependent mechanics of the material, the following assumptions can be made:

Transverse isotropic symmetry:

$$\begin{cases} E_2 = E_3 \\ \nu_{21} = \nu_{31} \\ \nu_{32} = \nu_{23} \\ G_{12} = G_{13} \\ G_{23} = \dfrac{E_2}{2 \times (1 + \nu_{23})} \end{cases} \tag{16}$$

Shear modulus is calculated thanks to Eq. (17), considering an elastic modulus for 0°, 45°, 90° and Poisson's ratio determined in the experimental study.

$$G_{12} = \frac{1}{\frac{4}{E_{45^\circ}} - \frac{1}{E_1} - \frac{1}{E_2} + 2\frac{\nu_{12}}{E_1}} \tag{17}$$

Time dependency does not depend on the material direction (as shown Fig. 13), Eq. (18) can be assumed:

$$\tau_1 = \tau_2 = \cdots = \tau_9 \tag{18}$$

A_i coefficients are defined from D_i identified in unidirectional tests.

$$\begin{cases} A_j = \dfrac{1}{\sum_{i=0}^{j-1} D_i} - \dfrac{1}{\sum_{i=0}^{j} D_i} \\ \sum_{i=0}^{N} A_i = \dfrac{1}{\sum_{i=0}^{N} D_i} \end{cases} \tag{19}$$

The problem's constitutive equations to be solved are as follows:

$$\begin{cases} \Delta\widetilde{\sigma} = \sum_{i=0}^{N} \Delta\widetilde{\sigma}_i \\ \Delta\widetilde{\sigma}_i = \widetilde{\widetilde{C}}_i^{-1} \left(\Delta\widetilde{\varepsilon} - \widetilde{\widetilde{\Gamma}}_i \widetilde{\sigma}_i(t) \times \Delta t \right) \\ \dfrac{\partial \Delta\widetilde{\sigma}}{\partial \Delta\widetilde{\varepsilon}} = \sum_{i=0}^{N} \widetilde{\widetilde{C}}_i^{-1} \end{cases} \tag{20}$$

Incremental viscoelastic strain is solved like Eq. (21).

$$\begin{cases} \Delta\widetilde{\varepsilon}_{an} = \left(\dfrac{\widetilde{\widetilde{\Gamma}}_i^{-1} \widetilde{\widetilde{C}}_i}{\Delta t} + \dfrac{1\widetilde{\widetilde{I}}}{2} \right) \left(\widetilde{\varepsilon}(t) + \dfrac{\Delta\widetilde{\varepsilon}}{2} - \widetilde{\varepsilon}_{an}(t) \right) \\ \widetilde{\varepsilon}_{an}(t + \Delta t) = \widetilde{\varepsilon}_{an}(t) + \Delta\widetilde{\varepsilon}_{an} \end{cases} \tag{21}$$

3.2.3. *Failure criteria to predict failure*

Finally, to predict creep failure, two failure indices for viscoelastic materials from the literature are introduced. Those have been successfully employed by Guedes[21] on experimental results by Myiano on carbon fiber-reinforced epoxy composites[20] to assess long-term viscoelastic failure. They were chosen for their ability not only to best fit experimental data, but also because they are the most penalizing compared to other indices[21].

The first one is based on a maximum strain criterion Eq. (22). It is simple to use but does not consider stress triaxiality.

$$MS_{index} = \max_{i,j \in [\![1,3]\!]} \left(\frac{\varepsilon_{ij}}{\varepsilon_{ij}^{rupt}} \right) \tag{22}$$

The second one is the Modified Reiner Weissenberg[37] index based on stored energy into material which takes into account stress triaxiality.

$$M - RW_{index} = \frac{W_s}{0,5 \times \max_{i,j \in [\![1,3]\!]} \left(\varepsilon_{ij}^{rupt} \times \sigma_{ij} \right)} \tag{23}$$

Where W_s is the stored energy, equal to the energy contained in springs of the model[21,31] and can be assessed for a constant unidirectional creep loading σ_0 as follows[31,37]:

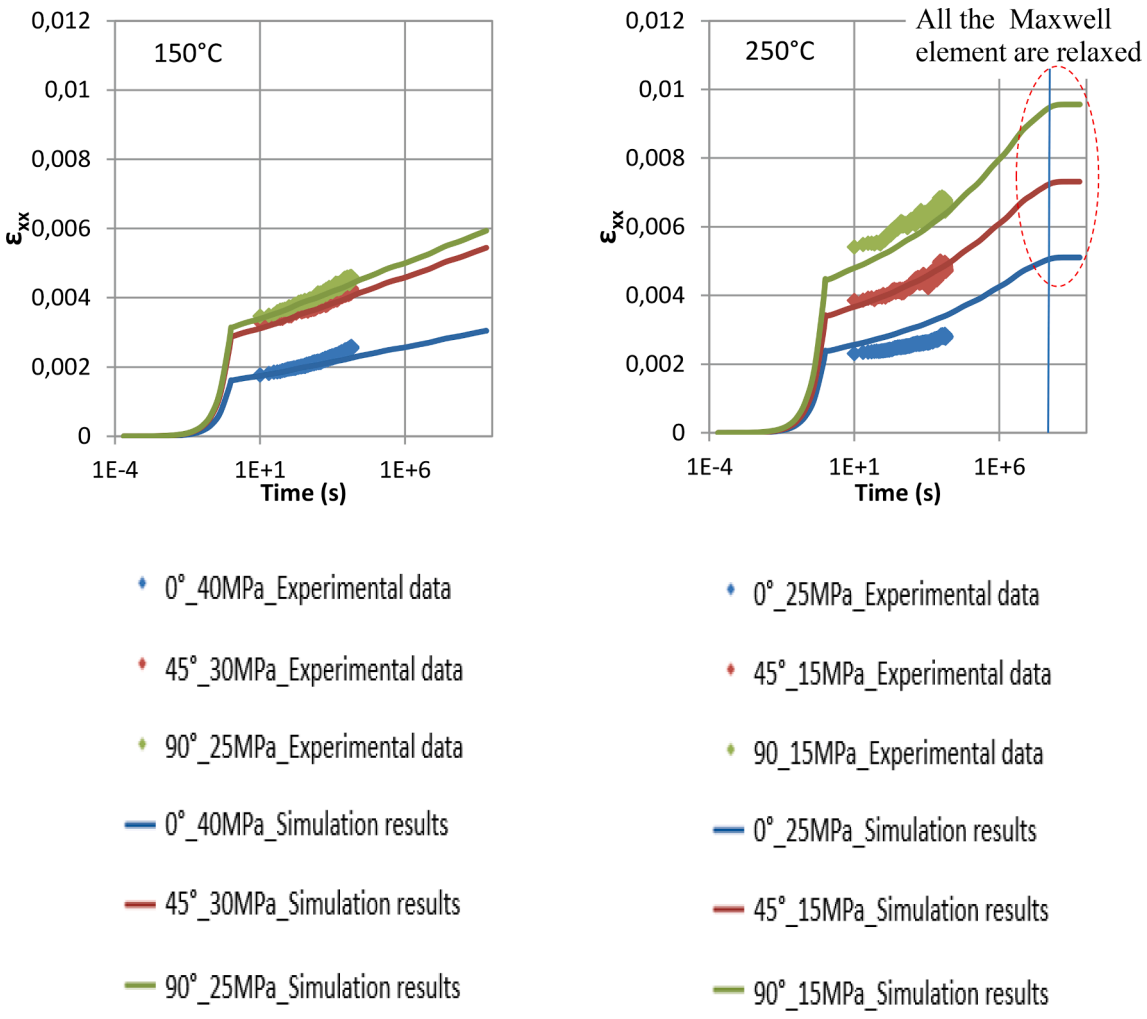

Fig. 25. Comparison of experimental data and simulation results according to fiber direction and temperature on a dogbone sample undergoing unidirectional creep for 20 years.

$$W_s = {\sigma_0}^2\left[\frac{D_0}{2}+\sum_{i=1}^{n}\frac{D_i}{2}\left(1-exp\left(-\frac{t}{\tau_i}\right)\right)^2\right] \tag{24}$$

The algorithm for calculation of a 3D part is described Fig. 18:

3.3. Results and discussion

From the experimental data and model proposed previously, the model will be identified, then a 3D model will be first validated and then used for calculation of an industrial part.

3.3.1. Identification 1D

From the experimental data and with Eq. (14), identification of the transient compliances D_i associated with the relaxation times τ_i can be computed. The method used consists in assuming $\tau_i = 10^{i-1}$ and solving Eq. (14) with a linear least squares solver *lsqlin* contained in Matlab. Relaxation times are chosen according to sampling rate (here 1 Hz, i.e. one datum is recorded every second) and experimental test duration (here, 4 h = 14400 s). The lowest relaxation time chosen must respect inequality $\tau_{min} < \frac{\Delta t}{3}$ as for smaller relaxation times, the associated maxwell element will be instantaneously relaxed. The highest relaxation time must be less than 3 times the total test duration: as for higher relaxation times, the associated Maxwell element will never be relaxed and will behave like a spring. In order to identify the model, the experimental data of the previously presented Fig. 10 are used. Results of the identification are shown in Fig. 19 and the parameters are summarized in Table 4. A very good description of the experimental data is obtained from the model. It can be observed that after 3 times the highest relaxation time (here, after 30000 s) the model saturates: evolution of creep compliance is no longer described. This is due to the fact that all of the model's Maxwell elements are then relaxed. If a longer simulation is carried out, transient compliances associated with longer relaxation times must be identified.

The model must therefore be identified over a long-time range, experimentally obtained by the time–temperature superposition principle (TTSP). The same procedure as previously on long-term experimental data shown Fig. 16 is computed, with relaxation times ranging from 10^{-30} to 10^{20}. The master curve is identified with less than 3.5% relative error (see Fig. 20).

3.3.2. Implementation and validation

Once identified on unidirectional experimental data, the model parameters are introduced into a user material subroutine (UMAT) developed for Abaqus simulation. In order to validate the model, some preliminary tests were conducted on a single hexahedral element (with 8 nodes, 3 degrees of freedom and 8 Gauss points – C3D8 in Abaqus) unidirectionally loaded (Fig. 21). An implicit algorithm is used in Abaqus. Loading is done within 1 s at 40 MPa under 150 °C and is maintained for 20 years or for 100 s before unloading.

Dependency upon the time increment is checked by changing it from 10^{-4}s to 10^{4}s. The conclusion is that the results are only weakly

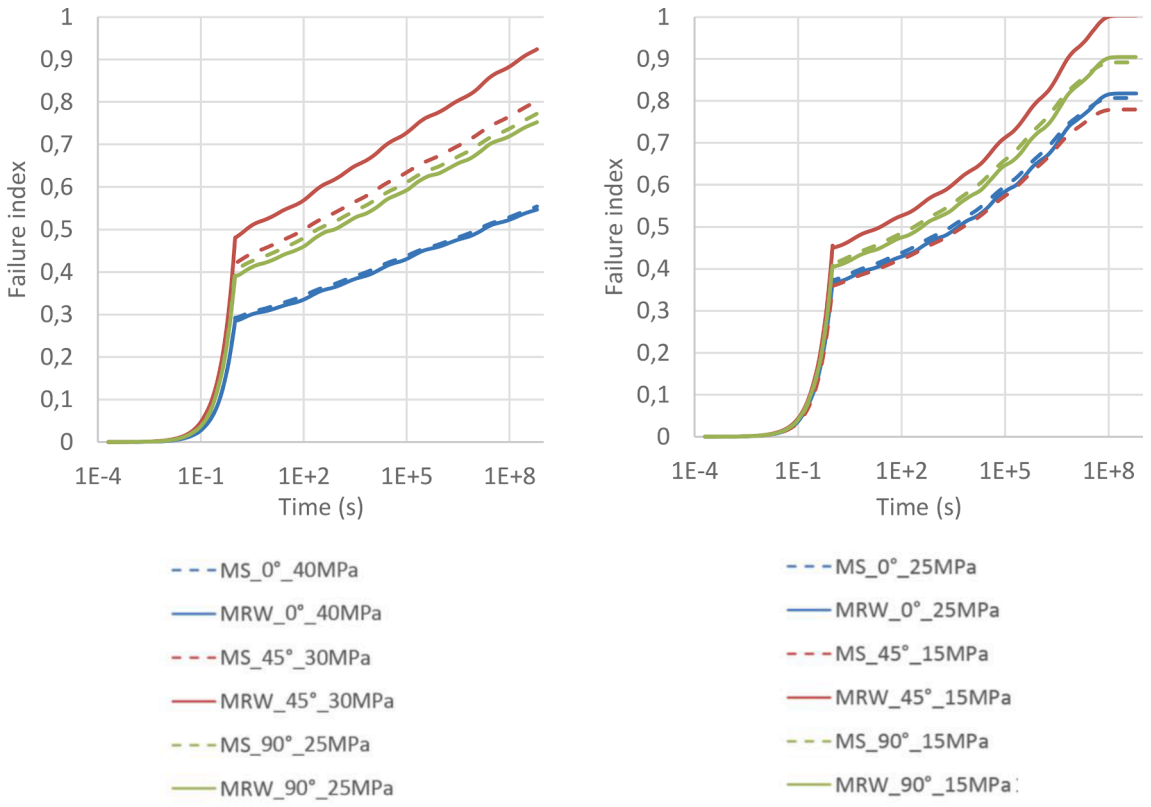

Fig. 26. Comparison of failure indices according to fiber direction and temperature on a dogbone sample undergoing unidirectional creep for 20 years.

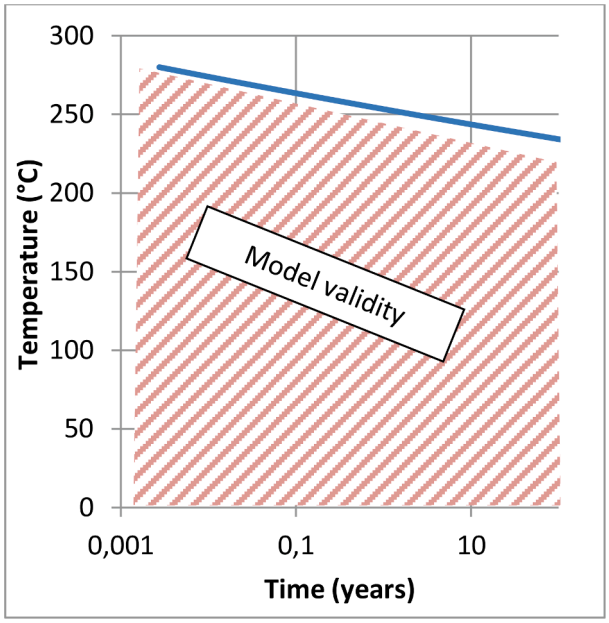

Fig. 27. Model validity according to temperature applied.

dependent on the time increment (less than 5%). Nevertheless, attention must be paid for complex loading paths including different loading steps. Simulation of the creep / recovery test shows poor results with the automatic increment. This can be explained by the inability of the model to take into account mechanical step change when it occurs between 2 times increments. Solution is to make time increment match the mechanical step change (i.e. to split time in as many steps as the mechanical path). The model leads then to satisfactory results (Fig. 22).

3.3.3. *Application of the model to structures*

Once the model has been identified and the methodology for calculation set, some simulations on structures can be carried out. We propose here to make some comparisons between simulation and experimental results on a dumbbell sample with different temperatures and fiber orientations. The sample is clamped at one of its ends and loaded with a point force on the other (Fig. 23 a.). Strain is measured inside the central zone of the sample where strain is homogeneous (Fig. 23 b.).

Simulations at 150 °C and 250 °C with material orientations of 0°, 45° and 90° for a stress equal to the damage threshold are carried out. Stress is applied within 1 s and maintained for 20 years (~6.3 10^8s). The increment is set to automatic, with a first increment value of 10^{-4}s and a maximum value of 10^7s.

Fig. 24 shows a comparison of experimental elastic modulus and elastic modulus obtained at the end of the loading step by the model. Both values are quite similar, leading mostly to an error of approximately 6%.

For long-term time-dependent behavior, Fig. 25 shows a comparison between simulation results and experimental data. The model identified from DMA data can now simulate material behavior whatever the temperature and whatever the fiber orientation as differences between simulations and experimental data remain limited. At 150 °C and for the longest times model tends to underestimate strain. This can be due to time-dependent damage or other non-linear behavior appearing during creep. At 250 °C, trends are consistent and results coherent. At 250 °C, trends are consistent and results coherent. However, simulation results at 250 °C show a decrease in strain rate, which reaches 0 s^{-1} after 4.95 10^7s (equivalent to 2.2 years). This is due to relaxation of all Maxwell elements. The model identified is limited by finite experimental data obtained.

The results of Maximum Strain (MS) and Modified Reiner Weissenberg (MRW) failure indices according to time, temperature and fiber orientation are shown in Fig. 26 for stress equal to the damage threshold. It is interesting to note that both failure indices are proportional to strain

evolution. The unidirectional stress state leads to similar values of MS and M−RW failure indices and is consistent with the work of Miyano [21]. We note that for 45° sample, MS and M−RW failure criterion give not the same values; M−RW criterion is higher than MS criterion. This is due to the fact that for this test, transverse and in-plane shear stresses are similar. So as the transverse strain at failure is lower than shear strain at failure, M−RW criterion is activated for transverse component although for MS criterion it is the shear strain. In fact MS criterion concern only strains, by M−RW is a coupled criterion between the strains and stresses corresponding then to a more predictive criterion. Finally, it is noted that for stresses below the damage threshold, failure indices do not predict part failure within 20 years, whatever the temperature and whatever the fiber orientation.

With the model identified and knowing the shift factor due to temperature, the validity of the model can be assessed as 3 times the maximum relaxation time of the model. As shown Fig. 27, the model can provide long-term calculation for a wide range of temperatures (more than 2 years at 250 °C, 25 years at 240 °C) which is good enough for most industrial applications.

4. Conclusion

In this study, very long-term creep behavior of an injection molded short carbon fiber-reinforced PEEK was investigated for stresses below the damage threshold, even for temperatures above glass transition temperatures. An experimental procedure, including creep/recovery tests and dynamic mechanical tests, was carried out to identify the time-dependent mechanical behavior and allow the choice of a model. The model parameters were identified thanks to experimental data obtained and some cross-tests were performed to demonstrate the confidence of the model obtained. Finally, the model was successfully used to simulate the time-dependent mechanical behavior of 3D parts.

Due to lack of large macromolecular movements, almost no creep appearings for temperatures below 120 °C. For higher temperatures, time-dependent mechanical behavior is linear viscoelastic for stresses below the damage threshold, even though little plasticity appears. Fiber orientation shows similar effects on linear viscoelasticity and on elasticity. Very long-term linear viscoelastic experimental data are obtained via dynamic mechanical analysis and the time temperature superposition principle, leading to satisfactory comparison with short-term creep data.

The Maxwell generalized model is suitable for unidirectional and three-dimensional calculation. Viscoelastic parameters are identified with experimental data and used as inputs for structure simulation. The model is implemented in Abaqus as a UMAT and simulation strategies were validated for long-term creep calculation and applied to a dumbbell sample by varying temperature and material orientations. Simulation results were compared with experimental data and provide satisfactory results. Failure criteria integrated into the model allow prevision of creep failure of structures. Finally, time/temperature limits for use of the model were defined.

Some experiments however, such as long-term creep, must be carried out to check the development of time-dependent damage or other time-dependent phenomena occurring over a long duration (viscoplasticity, aging etc.). These complementary data should provide a better time to failure estimation.

Declaration of Competing Interest

The authors declare that they have no known competing financial interests or personal relationships that could have appeared to influence the work reported in this paper.

References

[1] Aly NM. A review on utilization of textile composites in transportation towards sustainability. IOP Conf Ser Mater Sci Eng 2017;254:042002.
[2] Jacob A. Carbon fibre and cars – 2013 in review. Reinf Plast 2014;58:18–9.
[3] Díaz J. & Rubio L. Developments to manufacture structural aeronautical parts in carbon fibre reinforced thermoplastic materials. J. Mater. Process. Technol. 143–144, 342–346 (2003).
[4] Bessard, E. Matériaux Composites Structuraux à Base PEEK Élaborés Par Thermo-Compression Dynamique : Relation Procédé-Propriétés. (Ecole des mines d'Albi, 2012).
[5] da Costa AP, Botelho EC, Costa ML, Narita NE, Tarpani JR. A review of welding technologies for thermoplastic composites in aerospace applications. J Aerosp Technol Manag 2012;4:255–66.
[6] Shah SZH, Karuppanan S, Megat-Yusoff PSM, Sajid Z. Impact resistance and damage tolerance of fiber reinforced composites: A review. Compos Struct 2019;217:100–21.
[7] Sarasua JR, Pouyet J. Recycling effects on microstructure and mechanical behaviour of PEEK short carbon-fibre composites. J Mater Sci 1997;32:533–6.
[8] Willem van Ingen J, Buitenhuis A, van Wijngaarden M, Simmons III F. Development of the Gulfstream G650 induction welded thermoplastic elevators and rudder. Conf Pap 2010.
[9] Campo, E. A. Polymeric Materials and Properties. in Selection of Polymeric Materials 1–39 (Elsevier, 2008). doi:10.1016/B978-081551551-7.50003-6.
[10] Villoutreix J. Polyétheréthercétone (PEEK). Tech Ing 1998;13.
[11] Chang B, et al. Effects of temperature and fiber orientation on the tensile behavior of short carbon fiber reinforced PEEK composites. Polym Compos 2020. https://doi.org/10.1002/pc.25850.
[12] Berthet F, Lachaud F, Crevel J, Pastor M-L. Behaviour and damage of injected carbon-fibre-reinforced polyether ether ketone: From process to modelling. J Compos Mater 2017;51:141–51.
[13] Gao S-L, Kim J-K. Cooling rate influences in carbon fibre/PEEK composites. Part 1. Crystallinity and interface adhesion. Compos Part Appl Sci Manuf 2000;31:517–30.
[14] Ferry JD. Viscoelastic properties of polymers. Wiley; 1980.
[15] Schieffer A. Modélisation multiéchelle du comportement mécanique des composites à matrice organique et effet du vieillissement thermique. (Université Technologique de Troyes, 2003).
[16] Albouy W. De la contribution de la visco-élasto-plasticité au comportement en fatigue de composites à matrice thermoplastique et thermodurcissable. (INSA de Rouen, 2013).
[17] D'Amore A, Pompo A, Nicolais L. Viscoelastic effects in poly(ether ether ketone) (PEEK) and PEEK-based composites. Compos Sci Technol 1991;41:303–25.
[18] Endo VT, de Carvalho Pereira JC. Linear orthotropic viscoelasticity model for fiber reinforced thermoplastic material based on Prony series. Mech Time-Depend Mater 2017;21:199–221.
[19] Oseli A, Prodan T, Susič E, Slemenik Perše L. The effect of short fiber orientation on long term shear behavior of 40% glass fiber reinforced polyphenylene sulfide. Polym Test 2020;81:106262.
[20] Miyano Y, Nakada M, Nishigaki K. Prediction of long-term fatigue life of quasi-isotropic CFRP laminates for aircraft use. Int J Fatigue 2006;28:1217–25.
[21] Guedes RM. Creep and fatigue lifetime prediction of polymer matrix composites based on simple cumulative damage laws. Compos Part Appl Sci Manuf 2008;39:1716–25.
[22] Lévesque M. Modélisation du comportement mécanique de matériaux composites viscoélastiques non linéaires par une approche d'homogénéisation. (École Nationale Supérieure d'Arts et Métiers 2004.
[23] Cai H, Nakada M, Miyano Y. Simplified determination method of long-term viscoelastic behavior of amorphous resins. 18th Int Conf Compos Mater 2011.
[24] Guo Y, Bradshaw RD. Isothermal physical aging characterization of Polyether-ether-ketone (PEEK) and Polyphenylene sulfide (PPS) films by creep and stress relaxation. Mech Time-Depend Mater 2007;11:61–89.
[25] Nordin L-O, Varna J. Nonlinear viscoplastic and nonlinear viscoelastic material model for paper fiber composites in compression. Compos Part Appl Sci Manuf 2006;37:344–55.
[26] Maksimov RD, Kubat J. Time and temperature dependent deformation of poly (ether ether ketone)(PEEK). Mech Compos Mater 1997;33:517–25.
[27] Staub S, Andra H, Kabel M. & Zangmeister T. Multi-Scale Simulation of Viscoelastic Fiber-Reinforced Composites. 14.
[28] Hadid M, Rechak S, Zouani A. Empirical nonlinear viscoelastic model for injection molded thermoplastic composite. Polym Compos 2002;23:771–8.
[29] Crochon T. Modeling of the viscoelastic behavior of a polyimide matrix at elevated temperature. (Ecole polytechnique de Montréal, 2014).
[30] Vidal-Sallé E, Chassagne P. Constitutive equations for orthotropic nonlinear viscoelastic behaviour using a generalized Maxwell model Application to wood material. Mech Time-Depend Mater 2007;11:127–42.
[31] Miranda Guedes R. Mathematical Analysis of Energies for Viscoelastic Materials and Energy Based Failure Criteria for Creep Loading. Mech Time-Depend Mater 2004;8:169–92.
[32] Vincent M. Orientation des fibres courtes dans les pièces en thermoplastique renforcé. Tech Ing 2003;13.
[33] Deng S, Hou M, Ye L. Temperature-dependent elastic moduli of epoxies measured by DMA and their correlations to mechanical testing data. Polym Test 2007;26:803–13.

[34] Hanay, N. B. Treatise on Solid State Chemistry: Volume 3 Crystalline and Noncrystalline Solids. (Springer US, 1976).
[35] Golden HJ, Strganac TW, Schapery RA. An Approach to Characterize Nonlinear Viscoelastic Material Behavior Using Dynamic Mechanical Tests and Analyses. J Appl Mech 1999;66:872.
[36] Lai J, Bakker A. 3-D schapery representation for non-linear viscoelasticity and finite element implementation. Comput Mech 1996;18:182–91.
[37] Tanks J, Rader K, Sharp S, Sakai T. Accelerated creep and creep-rupture testing of transverse unidirectionalarbon/epoxy lamina based on the stepped isostress method. Compos Struct 2017;159:455–62.